

A planar micromachined spiral inductor for integrated magnetic microactuator applications

Chong H Ahn and Mark G Allen

Microelectronics Research Center, School of Electrical Engineering, Georgia Institute of Technology, Atlanta, GA 30332-0250, USA

Received 17 August 1993, accepted for publication 29 August 1993

Abstract. In this work, planar micromachined spiral inductive structures with relatively high inductance at low (Hz-kHz) frequencies are designed and fabricated for integrated magnetic microactuator applications and other purposes. Two types of multilayer micromachined inductors have been investigated. The first structure is a standard planar inductor spiral. To this structure we have added an electroplated high-permeability nickel-iron (Ni/Fe) magnetic core, which forms a central core to concentrate flux and completely encapsulates the windings, thus minimizing magnetic interference. For a typical 36-turn device 3 mm \times 3 mm in area, an inductance of approximately 20 μ H was obtained. The structure with a magnetic core has an inductance four to five times greater than a similar structure without a magnetic core. The specific inductance of our structure (inductance per unit area) is 2.2 μ H mm⁻² at 10 kHz, which is one of the highest inductance values ever achieved in an integrated planar inductive component at low frequency. Since the structure of the spiral-type inductor is similar to those of planar magnetic microactuators such as micropumps, microvalves and microrelays, several low-frequency microactuator applications are expected to be possible with this inductor.

1. Introduction

Integrated-circuit-compatible thin-film inductors have application in areas such as filters, oscillators, low-power converters, and on-chip generation of magnetic fields for magnetic microactuation. One difficulty with these structures, however, is the relatively low inductances which can be achieved, typically of the order of hundreds of nanohenries (nH) to several microhenries (μ H). Due to the relatively low values of inductance, most previously fabricated structures have been operated in the very-high-frequency regime, for example as passive components in microwave circuits.

Several spiral-type inductive components have been reported previously. In these structures, spiral conductors are placed on an insulated substrate [1-3], a magnetic substrate [4,5], or between top and bottom magnetic thin films [6]. Due to the geometrical characteristics of the spiral, the fluxes generated in the absence of magnetic cores will be spread throughout the surface of the substrate. These fluxes are composed of two components which are either parallel or perpendicular to the surface [3]. Accordingly, it is difficult to guide the magnetic flux to a specific point in such a structure without using a magnetic core. Such

flux guidance is required for magnetic microactuators such as those realized recently [7,8].

One of the earlier applications of the spiral-type inductive components was integrated magnetic recording heads, which have been investigated since the 1970s. In the magnetic head, a stack of spiral conductors is deposited on the magnetic core layer, on top of which magnetic layers are successively deposited to build magnetic legs, completing a closed magnetic circuit through the gaps [9,10]. However, the magnetic heads have been optimized for non-actuator applications, and may not have the required flux generation capability and/or current carrying capability for magnetic microactuators.

Recently, new micromachining techniques have enabled the realization of integrated inductive components [11,14,16], magnetic microactuators [12-14], and magnetic micropower devices [15,16] which are fabricated on a silicon substrate. There have been demands for new micromachined integrated inductive components which can be operated at low frequencies and have high inductance for magnetic flux generation as well as magnetic energy storage. In magnetic micropower devices such as integrated DC/DC converters or magnetic microactuators using a spiral inductor, many coil turns

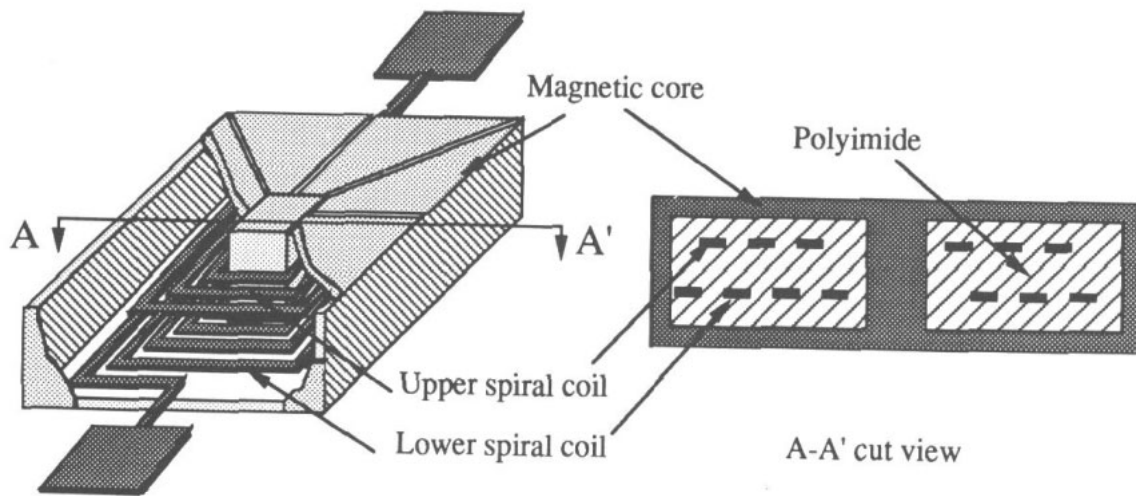


Figure 1. Schematic diagram of a spiral-type inductive structure which has a closed magnetic circuit and a thick conductor line.

are required to achieve a high inductance and a high magnetic flux density, which significantly increases the resistance of the conductor coils due to the increased coil length. Thus, the usefulness of this structure as a basic inductive component for magnetic microactuator applications depends on how the resistance of the conductor coils can be reduced, while achieving low reluctance in the magnetic circuits. Although a few magnetic microactuators with spiral inductive geometry without magnetic cores have been reported [7, 8], such inductive structures cannot easily guide flux to a single point for microactuator applications.

There are two major difficulties that must be overcome in order to improve the usefulness of this geometry. First, closed magnetic circuits must be completed using a thick magnetic material with high permeability to reduce magnetic reluctance and to minimize magnetic field interference (making the adhesion of the thick magnetic layer a concern). Second, the spiral conductor must have as small a resistance as possible to reduce power consumption in the conductors.

In the work described in this paper, these limitations have been overcome by using micromachining fabrication techniques to build a spiral-type inductive component that is composed of completely closed magnetic circuits and thick conductor lines. The magnetic flux generated from the spiral coils is confined by the closed magnetic circuit, which ensures better flux linkage between spiral coils and the magnetic circuit, thus resulting in a maximum inductance and minimum electromagnetic field interference (EMI). Considering the magnetic flux path in the spiral inductor, which is encapsulated with magnetic cores, the magnetic flux produced from the spiral coils will be concentrated at the centre core pole, flowing through the bottom core (or the top core), the outer core cylinder, and the top core (or the bottom core) in the series. If a small air gap is introduced between the top core and the centre core pole, magnetic force can be generated at the air gap when a current

is applied to the spiral coils. Fortunately, air gaps and movable mechanical structures can be easily inserted in this structure as part of the magnetic circuit by using surface micromachining techniques and sacrificial layers. If the top core is released from the top of the centre core pole as a movable membrane or a deflectable cantilever beam, several planar microactuator applications of this inductor such as micropumps, microvalves, and microrelays are to be expected due to their structural similarities. Because of the large core reluctance in magnetic microactuators, the magnetic reluctance due to a small air gap inserted in the closed magnetic circuit is usually comparable to or less than magnetic core reluctance [12, 14]. Thus, the air gap inserted in this geometry may not break the tight flux linkage between the coils and the magnetic circuits, consequently reducing EMI.

2. Device concept and model

The major concerns in designing this type of inductor are to achieve a high inductance, a low coil resistance, and a low magnetic field interference, thereby maintaining a high Q factor. Increasing the number of spiral turns increases the inductance; a multilayer approach to increase the number of turns can be used. Upper and lower spirals are connected through a metal via connection in order to construct the double-layered planar spiral coils. If magnetic cores with a high permeability encapsulate double-layer spiral coils, thus constructing a closed magnetic circuit, the inductance value achieved is increased due to the low reluctance of the interlinked magnetic circuit between coils and cores. Accordingly, the magnetic field interference can be minimized, confining the magnetic fluxes to the closed magnetic circuit. A spiral structure design to satisfy these requirements is shown in figure 1, where spiral conductance lines are completely encapsulated

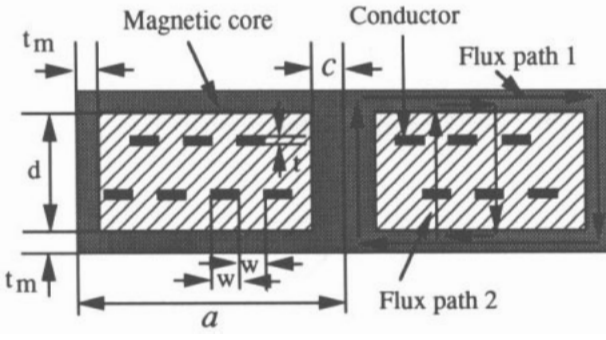


Figure 2. Schematic diagram of spiral inductor to be modeled.

by an electroplated thick nickel-iron permalloy, thus closing the magnetic circuit.

Kimura *et al* [17] have presented a simplified model of double spiral coils for the inductance calculation of the closed outer core. Figure 2 shows a schematic diagram of the inductor to be modeled to determine its inductance value. Two paths of magnetic flux are generated from the i th coil current in this model: one is through the closed magnetic core, which confines the parallel component of generated magnetic field to the surface; the other encloses the i th coil through the air gap located between the upper and lower cores, which confines the vertical component of the generated magnetic field to the surface. To calculate the mutual inductance that exists between the i th and j th coils, a magnetic reluctance for the first path, path 1, is defined as R_1 . The magnetic reluctances for the second, path 2, in terms of the i th and j th coils are defined as R_{ij1} for $i \leq j$ and R_{ij2} for $i \geq j$ respectively. If the double spiral layers have N spiral turns on each level, the inductance L_1 in path 1 is given as:

$$L_1 = (2N)^2 / R_1. \quad (1)$$

The inductance, L_2 , in path 2 is expressed as:

$$L_2 = 4 \sum_{j=1}^N \left(\sum_{i=1}^j \frac{1}{R_{ij1}} + \sum_{i=j+1}^N \frac{1}{R_{ij2}} \right). \quad (2)$$

The internal self-inductance of the coil, L_i , can be written as:

$$L_i = (\mu_0 / 4\pi) l_i / 2 \quad (3)$$

where l_i denotes the total length of the double-layer coil which can be simply defined from figure 2 as:

$$l_i = 2 \left\{ 3(2c + 4w) + \sum_{i=0}^{(2N-1)} \left[(2c + 4w) + 2w(i-1) \right] \right\}. \quad (4)$$

Finally, the total inductance L obtained from the summation of these inductances can be expressed as:

$$L = L_1 + L_2 + L_i. \quad (5)$$

It is useful to substitute typical micromachining geometries into the above model. For $a = 1346 \mu\text{m}$, $c = 508 \mu\text{m}$, $d = 30 \mu\text{m}$, $N = 18.5$, $t_m = 8 \mu\text{m}$,

Table 1. Electrical parameters measured and evaluated from different geometries of spiral inductor. The device types refer to differing design parameters of the inductors.

Geometry	A-type	B-type	C-type
N (turns)	18	21	14.5
a (μm)	1346	4139	5270
c (μm)	508	1586	2348
d (μm)	30	30	30
t_m (μm)	8	10	10
w (μm)	12.5	50	62.5
l_1 (μm)	532	1687	2474
μ_r	200	200	200
L_{eval} (μH)	24.71	40.95	21.33
L_{meas} (μH)			
(at 10 kHz)	20.0	20.5	13.5
R_{eval} (Ω)	200.4	180.5	123.15
R_{meas} (Ω)			
(at 10 kHz)	295.3	214.8	142.9

and $w = 12.5 \mu\text{m}$, the evaluated inductances are $L_1 = 14.5 \mu\text{H}$, $L_2 = 10.2 \mu\text{H}$, $L_i = 0.01 \mu\text{H}$, and $L = 24.71 \mu\text{H}$, where a relative permeability of 200 is assumed. From these calculated values, it is interesting to note that the inductance value resulting from path 2, including the air gaps, has a value almost comparable to that resulting from path 1 through the closed magnetic circuits. The inductance values evaluated from different geometries of the spiral inductor using this model are listed in table 1.

The resistance of the double-layered spiral coils can be calculated using the total spiral length from equation (4),

$$R = \rho l_i / wt \quad (6)$$

where ρ is the resistivity of the conductor which is assumed to be approximately $3.5 \mu\Omega \text{ cm}$, w and t denote the width and the thickness of conductor respectively. The resistance evaluated from equation (6) is about 202.5Ω .

From equations (5) and (6), the Q factor of this inductor can be expressed as:

$$Q = \omega L / R. \quad (7)$$

From (6) it is evident that when the thickness of the conductor lines is increased, the conductor resistance is reduced. Also, L_1 and L_2 are not greatly affected by gap variation between the upper and the lower cores resulting from variation of conductor thickness. As a result, the increase in Q -factor resulting from increasing the conductor thickness is due mainly to the decrease of conductor resistance. Unfortunately, the achievable double-layered spiral conductor thickness is fabrication-limited, since the thick conductors produce a poor surface planarization which causes difficulties in the photolithography process for the next layer. The relationship between the conductor thickness and the Q -factor using the equations above are shown in figure 3, which shows that the Q -factor increases almost linearly as the thickness of the conductor is increased.

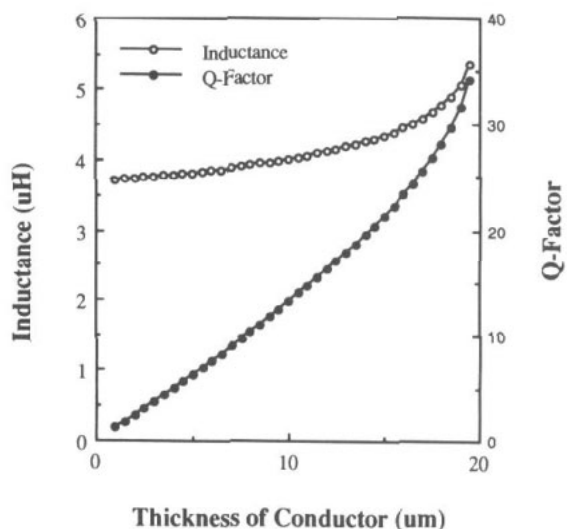


Figure 3. Inductance and Q -factor calculated as a function of conductor thickness, which shows that the Q -factor is increased almost linearly as the thickness of the conductor is increased.

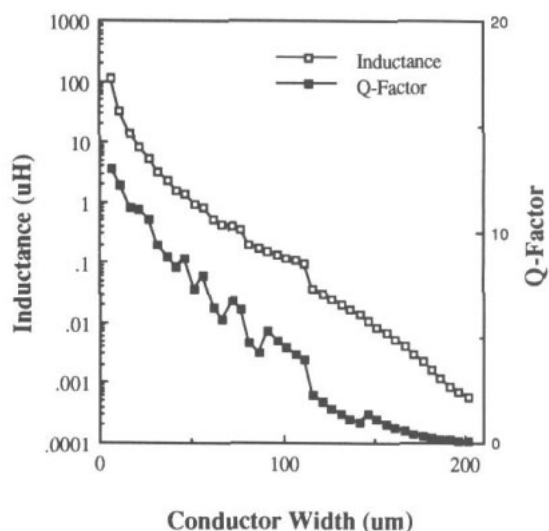


Figure 4. Inductance and Q -factor calculated as a function of conductor width W for a fixed inductor area. The roughness in the above curves reflects the discrete quantization of the number of conductor turns as W is varied.

If the thickness of the closed magnetic core is increased, the resulting inductance value L_1 is also increased, since the magnetic reluctance in path 1 is decreased. The Q -factor is affected by L_1 , since it is a function of the thickness of the closed magnetic core. From this evaluation, it is found that both the inductance value and the Q -factor increase when the thickness of the magnetic core is increased.

When a planar inductive component is fabricated monolithically with integrated circuits, the area occupied by the planar inductive component must be limited. In a given area (i.e. for the given length of a in this model), the number of spiral-coil turns and the resistance are varied as the conductor width (w) is changed. The dimension of the center magnetic core (i.e. defined as c in this model) also affects the area that can be occupied by the conductors. Using equations (6)

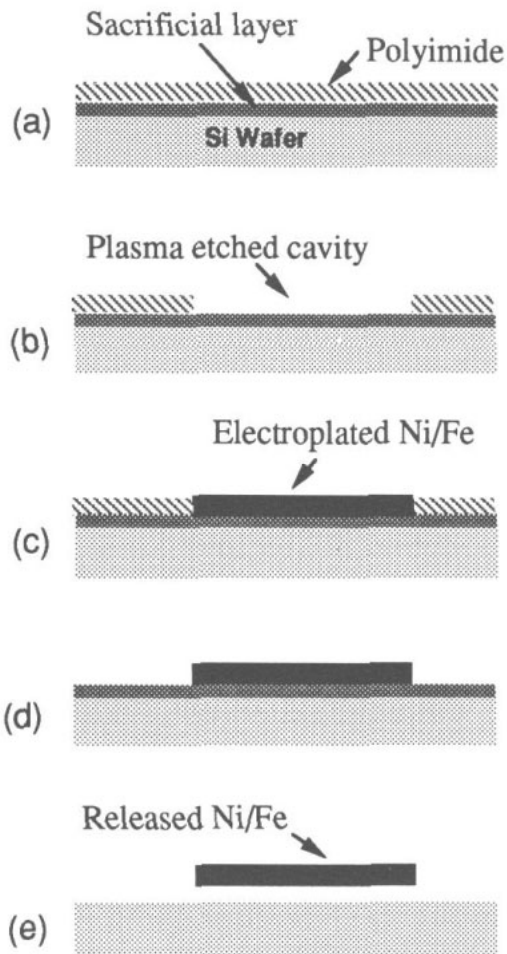


Figure 5. Fabrication sequence of the test samples for the *in situ* measurement of magnetic properties: (a) sacrificial layer and polyimide deposition; (b) cavity etching; (c) Ni-Fe plating; (d) polyimide etching; (e) Ni-Fe release.

and (7), Q -factors can be evaluated by changing w for the fixed area, and this is plotted in figure 4. From this evaluation it is verified that the Q -factor has a larger value for smaller conductor widths. The inductance value is proportional to the square of the number of coil turns (i.e. the square of the width variation) but the resistance is linearly proportional to the width variation. To find the maximum Q -factor for a conductor width w at the optimized dimension of c , w is varied from $2 \mu\text{m}$ to a quarter of a (which ensures at least two spiral turns). The Q -factor has maximum values at around $c = 216 \mu\text{m}$ and $w = 100 \mu\text{m}$ for a typical device $3 \text{ mm} \times 3 \text{ mm}$ in area.

The following considerations affect the choice of dimensions to achieve a maximized Q -factor for a given area: (i) the Q -factor increases with the conductor thickness; (ii) the Q -factor increases with the core thickness; (iii) the Q -factor increases as the conductor width decreases; (iv) there is an optimal conductor width for a given center core width and area.

3. Magnetic material deposition and characterization

In designing a planar inductive component, magnetic material properties measured from bulk-type magnetic

Table 2. Composition of the Ni-Fe electroplating solution.

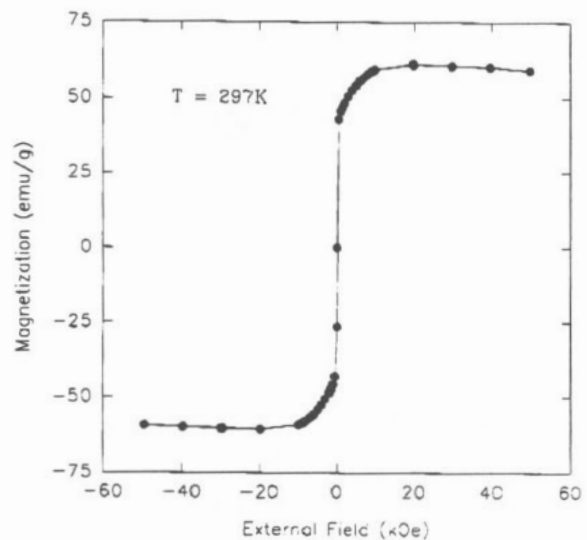
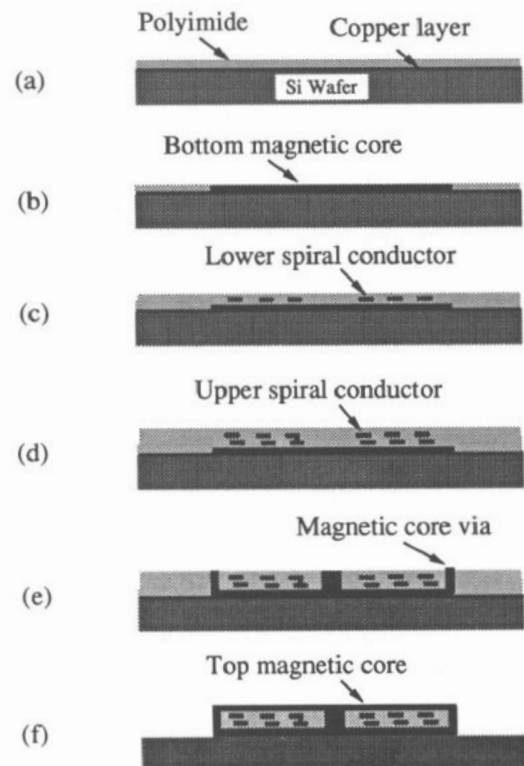
Component	Quantity (g l ⁻¹)
NiSO ₄ ·6H ₂ O	200
FeSO ₄ ·7H ₂ O	8
NiCl ₂ ·6H ₂ O	5
H ₃ BO ₃	25
Saccharin	3

samples may not be useful since the magnetic properties may depend on film geometry, thickness, and size. Thus, before designing a planar inductor, the magnetic properties of the thin film-type core should be understood. In measuring the properties of a magnetic film used for micromagnetic structures, it is important to remember that the properties of interest must be measured *in-situ*; that is, on as-deposited films.

Of the soft magnetic materials available, nickel-iron permalloy has been identified as a promising magnetic material and has been used in a variety of magnetic film applications, since it has favorable magnetic [18,19] as well as mechanical [20] properties. In particular, the Ni (81%)/Fe(19%) composition film can meet the requirements for magnetic microactuator applications, because this composition allows the simultaneous achievement of maximum permeability, minimum coercive force, minimum anisotropy field, and maximum mechanical hardness. Ni(81%)/Fe(19%) permalloy can be deposited by using either evaporation or electroplating; in this research the latter technique is adopted due to the cost advantage in making a film of several tens of μm in thickness. A plating bath was built using the compositions shown in table 2 [18–19].

Test samples were prepared using surface micro-machining techniques to meet the *in-situ* measurement requirement. The fabrication sequence used, which is similar to the fabrication steps described later in this paper, is shown in figure 5. This fabrication was performed using the fabrication mask sets also to be used in the fabrication of actual magnetic components. Thus, the prepared test samples had exactly the same sizes and the geometries as the magnetic films used in the micromachined magnetic components. The geometry of test samples prepared for *in-situ* measurement in this research was of thin-film type, and the same as that of the bottom magnetic core of the inductor to be fabricated.

The measurements of the material B - H curves were obtained from magnetization versus applied field curves obtained using a susceptometer-magnetometer (model 7225, Lake Shore Cryotronics Inc). Figure 6 illustrates the results of the high-field measurements for the thin-film type geometry. From the B - H values calculated from the values shown in figure 6, the thin-film type magnetic core is saturated at approximately 0.65 T and the evaluated relative permeability μ_r is approximately 150–300 in the linear region. We have measured μ_r from 100–900 using this technique. It should be emphasized that the above calculation assumes zero demagnetization effect. Note that

**Figure 6.** Magnetization (emu g^{-1}) as a function of applied dc field (Oe) using the high-field measurements for the thin-film type core.**Figure 7.** Fabrication sequence of the planar-spiral inductive component: (a) polyimide deposition; (b) bottom magnetic core plating; (c) patterning lower spiral conductor; (d) patterning upper spiral conductor; (e) magnetic core wall plating; (f) top magnetic core plating.

the relative permeability and flux saturation at high frequencies may have different values from those obtained at low frequencies in this section.

4. Fabrication

The fabrication steps of this component are shown in figure 7. The process started with oxidized ($0.6 \mu\text{m}$)

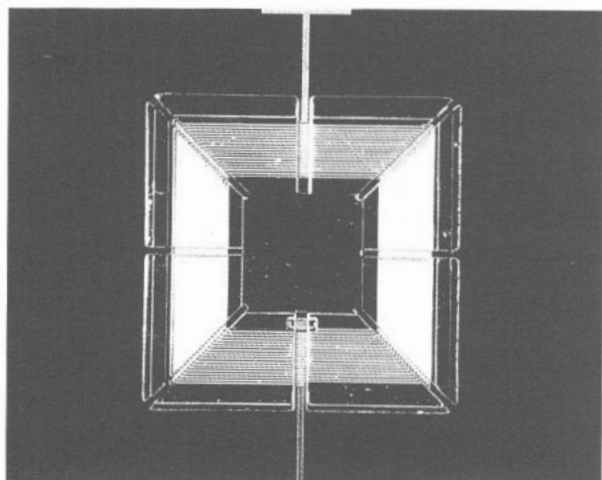


Figure 8. Photomicrograph of the fabricated planar-spiral inductive component with an encapsulating magnetic core.

three-inch (100) silicon wafers as a substrate. Onto this substrate, 2000 Å of titanium was deposited as an electroplating seed layer using DC sputtering. Polyimide (Dupont PI-2611) was then spun onto the wafer to build electroplating molds for the bottom magnetic core. Three coats were used to obtain a thick polyimide film. Each coat was cast at 3000 rpm, and soft baked for 10 min at 120 °C prior to the application of the next coat. After the deposition of all coats, the polyimide was cured at 350 °C for 1 h in nitrogen, yielding an after-cure thickness of 9 μm. Holes were etched in this polyimide using a 10% CF₄/O₂ plasma etch and an aluminium hard mask until the titanium seed layer was exposed. The electroplating forms were then filled with a Ni(81%)/Fe(19%) permalloy using standard electroplating techniques and the Ni-Fe electroplating bath described in table 2. To electroplate the bottom magnetic cores, electrical contact was made to the seed layer, and the wafers were immersed in the plating solution. During the electroplating, the solution was maintained at room temperature and a pH of approximately 2.7, and was stirred very slowly with a Teflon propeller blade. An applied current density of 5 mA cm⁻² resulted in a electroplating rate of 0.3–0.4 μm min⁻¹. In order to insulate the bottom magnetic core from the conductor coil, polyimide was spin-coated (as above) at 4000 rpm, and hard-cured at 350 °C for 1 h.

For the lower spiral conductor, 7 μm of aluminium was DC sputtered onto the polyimide and patterned using conventional lithography and phosphoric-acetic-nitric (PAN) aluminium etching solution. In order to insulate the conductor line and replanarize the surface, more polyimide was deposited in multiple coats (as described above). Two coats of polyimide were deposited and cured as described above, yielding approximately 6 μm of polyimide. To connect the lower spiral coils to the upper spiral coils, a via hole was then dry-etched through the polyimide layer using 100%

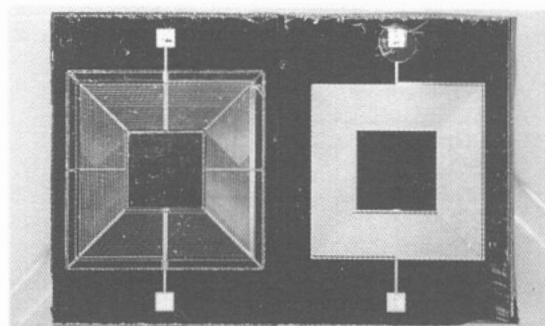


Figure 9. Photomicrograph of the inductive components with (left side) or without (right side) a magnetic core, where both components are fabricated simultaneously on the same substrate.

oxygen plasma and an aluminium hard mask. After removing the aluminium hard mask, 7 μm of aluminium was DC sputtered and patterned again as described for the lower spiral coils. Two coats of polyimide were deposited and cured, achieving an insulator for the conductor and a planarized surface.

To complete a closed magnetic circuit, magnetic vias were etched both at the center and at the outside of the spiral coils using the same technique as described above. Upon completion of the via etch, the surface of the magnetic core was oxidized because the bottom magnetic core was exposed to the oxygen plasma during dry etching. To remove the oxide film, the exposed areas of the bottom magnetic cores were etched in a 2% hydrofluoric acid solution for 30 s. Contact was then made to the bottom magnetic core, and the vias were filled with Ni-Fe using the electroplating bath and conditions described previously. Upon completing of the electroplating, the magnetic vias were coated with a single layer of polyimide spun on the wafer at 5000 rpm and cured.

The top magnetic core was then plated over the magnetic vias, completing the magnetic circuit. To electroplate the top cores, an evaporated nickel seed layer was defined between the magnetic vias using a lift-off technique. After the construction of the photoresist plating mold, top magnetic cores were plated using the electroplating conditions described above. Bonding pads were then opened through polyimide layers for the electrical test using the via etch process sequence described earlier. The photomicrographs of the fabricated spiral inductive components with or without an encapsulating magnetic core are shown in figures 8 and 9 respectively. The scanning electron micrograph of the structure with a magnetic core is shown in figure 10, which was taken after dry-etching of the polyimide. Finally, samples were diced into chips for bonding and testing as shown in figure 11.

5. Device performance

For a typical 36-turn device 3 mm × 3 mm in area, an inductance of approximately 20 μH was obtained at 10 kHz. A plot of inductance versus frequency

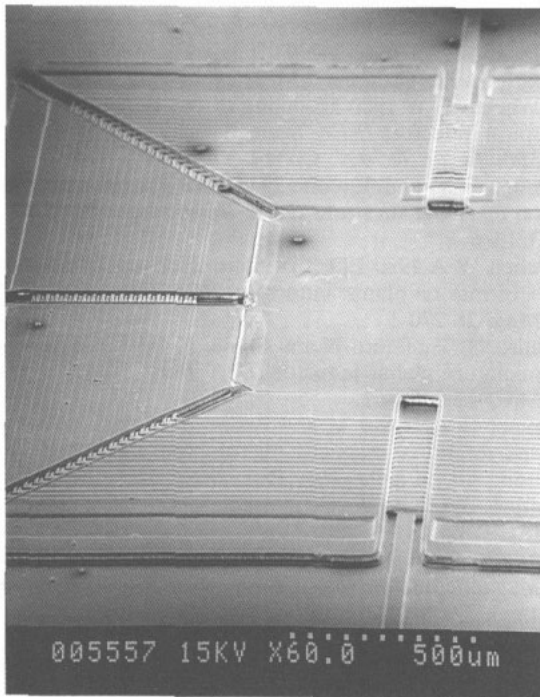


Figure 10. Scanning electron micrograph of a section of the fabricated spiral-type inductor with a magnetic core.

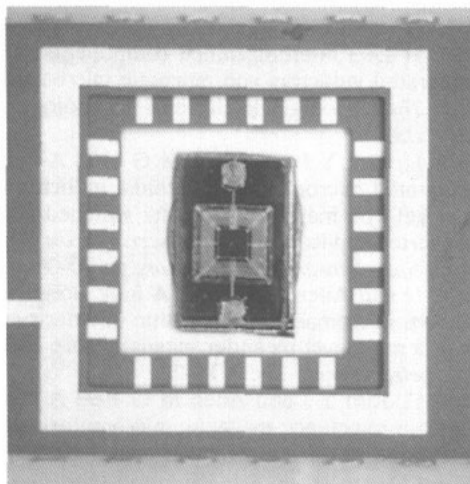


Figure 11. Photomicrograph of the fabricated inductor mounted on the chip carrier.

for two planar spiral inductor structures, one with a magnetic core and the other without a magnetic core, is shown in figure 12. The magnetic core has increased the inductance by a factor of 4–5 compared with the structure without the magnetic cores. The obtained inductance of $2.2 \mu\text{H mm}^{-2}$ at 10 kHz is one of the highest inductance values that has been achieved in an integrated planar inductive component. It should be noted that the increase in inductance falls off at frequencies above 3 MHz, presumably due to the decreasing permeability of the Ni-Fe permalloy at higher frequencies. To reduce the conductor resistance, aluminium was deposited using DC sputtering to a thickness of $7 \mu\text{m}$, which still allowed subsequent planar

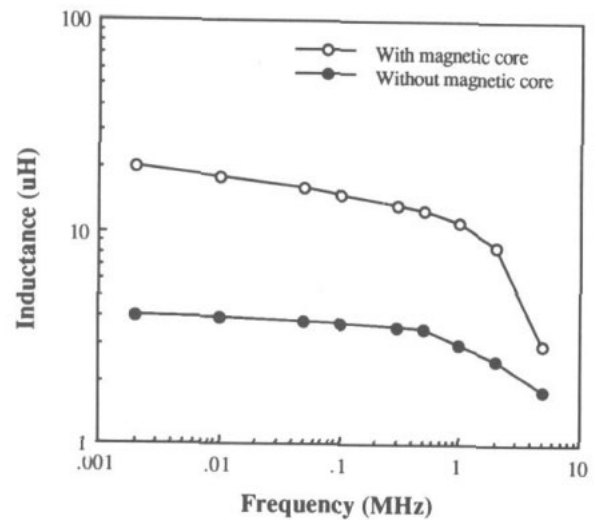


Figure 12. Measured inductance with magnetic cores or without any magnetic material as a function of frequency.

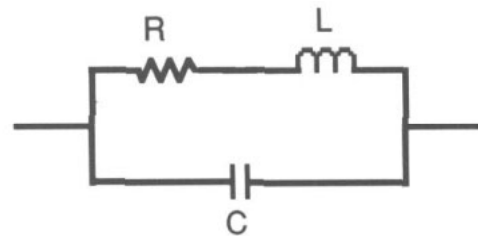


Figure 13. Equivalent circuit of the spiral-type inductor for electrical parameter evaluation.

processing without any difficulty. Double layers of spiral coils were connected through a metal via contact to increase the coil turns. In spite of the conductor thickness, the measured conductor resistance was still as high as approximately 300Ω which disagrees with the calculated value of 200Ω . This discrepancy is presumably due to high via contact resistance as well as long conductor leads to the bonding pad. There are several factors which determine the Q value of miniaturized inductive components encapsulated by a magnetic core. As evaluated in the previous section, Q values are affected by conductor thickness and width and by the thickness of the magnetic core. The optimized geometric values for a maximum Q factor from the previous section will be useful in the design of this inductive component. The achievable maximum Q factor at low frequencies around 10 kHz from the optimized geometry is expected to be 10–20. However, in realizing an actual magnetic microactuator using the spiral inductor with magnetic cores, the highest Q factor may not be as important as the lowest conductor resistance.

In order to evaluate the capacitance of the inductor, an equivalent circuit was assumed as shown in figure 13, and the resistance and stray capacitance of the inductor were derived from the measured impedance and phase as a function of frequency using equivalent circuit analysis. From this analysis for a typical 36-turn, $3 \text{ mm} \times 3 \text{ mm}$ inductor, the stray capacitance was shown to be in the several tens of picoFarads, and to have a

negligibly small effect over the low frequency ranges used. The electrical parameters measured and evaluated from different geometries of spiral inductor are listed in table 1, and are compared with the values predicted by the device model described earlier. Theory and experiment show a reasonable match in the smaller sized devices, but the discrepancy slightly increases as the size of the inductor is increased.

6. Conclusions

In this work we have designed and fabricated planar micromachined inductive components with relatively high inductance at low (Hz–kHz) frequencies for integrated magnetic microactuator applications and other purposes. Two types of multilayer micromachined inductors have been investigated. The first structure is a standard planar inductor spiral without a magnetic core. We have added to this structure an electroplated high-permeability Ni–Fe central magnetic core, which concentrates flux and completely encapsulates the windings, thus minimizing magnetic interference. For a typical 36-turn device 3 mm × 3 mm in area, an inductance of approximately 20 μH was obtained. The presence of a magnetic core increases the inductance with respect to similar structure without a magnetic core by a factor of 4–5. This increase, although significant, is less than expected due to the winding-to-winding leakage flux. It should also be noted that the increase in inductance falls off at higher frequencies, presumably due to the decreasing permeability of the Ni–Fe core at high frequencies. The specific inductance of this structure (inductance per unit area) is 2.2 $\mu\text{H mm}^{-2}$ at 10 kHz, which is one of the highest inductance values achieved in an integrated planar inductive component at low frequency.

Acknowledgments

This work was supported in part by the National Science Foundation under grant ECS-9117074. The authors would like to gratefully acknowledge Dupont and OCG Microelectronic Materials for their donations of polyimide and Lake Shore Cryotronics, Inc. for their assistance in measurements of the magnetic properties of the permalloy in thin films. The fabrication was performed in Microelectronics Research Center at the Georgia Institute of Technology.

References

- [1] Olivei A 1969 Optimized miniature thin-film planar inductors compatible with integrated circuits *IEEE Trans. Part, Mater. Packaging* PMP-5 71–88
- [2] Greenhouse H M 1974 Design of planar rectangular microelectronic inductors *IEEE Trans. Part, Hybrids Packaging* PHP-10 101–9
- [3] Rodriguez R, Dishman J M, Dickens F D and Whelan E W 1980 Modeling of two-dimensional spiral inductors *IEEE Trans. Components, Hybrids, Manufactur. Technol.* CHMT-3 535–41
- [4] Roshen W A and Turcotte D E 1988 Planar inductors on magnetic substrate *IEEE Trans. Magn.* MAG-24 3213–6
- [5] Roshen W A 1990 Effect of finite thickness of magnetic substrate on planar inductors *IEEE Trans. Magn.* MAG-26 270–5
- [6] Oshiro O, Tsujimoto H and Shirae K 1987 A novel miniature planar inductor *IEEE Trans. Magn.* MAG-23 3759–61
- [7] Wagner B, Kreutzer M and Benecke W 1992 Linear and rotational magnetic micromotors fabricated using silicon technology *Proc. IEEE Micro Electro Mech. Sys. Workshop (Germany, 1992)* (New York: IEEE) pp 183–9
- [8] Yanagisawa K, Tago A, Ohkubo T and Kuwano H 1991 Magnetic microactuator *Proc. 4th IEEE Workshop on Micro Electro Mech. Sys. (Nara, Japan, 1991)* (New York: IEEE) pp 120–4
- [9] Miura Y, Takahashi T, Kume F, Toda J, Tsutsumi S and Kawakami S 1980 Fabrication of multi-turn thin film head *IEEE Trans. Magn.* MAG-16 779–881
- [10] Noro Y, Ohshima I, Saito M, Yamada M and Tanaka K 1982 Fabrication of multitrack, thin-film head *J. Appl. Phys.* 53 2611–3
- [11] Ahn C H and Allen M G 1994 A new toroidal-meander type integrated inductor with a multilevel meander magnetic core *IEEE Trans. Magn.* at press
- [12] Ahn C H 1993 Micromachined components as integrated inductors and magnetic microactuators *PhD Thesis* Georgia Institute of Technology, Atlanta, GA, USA
- [13] Ahn C H, Kim Y J and Allen M G 1993 A fully integrated micromachined toroidal inductor with a nickel-iron magnetic core (the switched DC/DC converter application) *Transducers 6th Int. Conf. Solid-State Sensors and Actuators* pp 70–3
- [14] Ahn C H and Allen M G 1993 A fully integrated surface micromachined magnetic microactuator with a multilevel meander magnetic core *IEEE J. Microelectromech. Sys.* 2 15–22
- [15] Ahn C H, Kim Y J and Allen M G 1993 A planar variable reluctance magnetic micromotor with fully integrated stator and wrapped coils *Proc. IEEE Micro Electro Mech. Sys. Workshop (Fort Lauderdale, FL, 1993)* (New York: IEEE) pp 1–6
- [16] Mino M, Yachi T, Tago A, Yanagisawa K and Sakakibara K 1992 A new planar microtransformer for use in micro-switching converters *IEEE Trans. Magn.* MAG-28 1969–73
- [17] Kimura M, Miyakoshi N and Diabow M 1991 A miniature opto-electric transformer *Proc. IEEE Microelectromechanical Sys. Workshop* (New York: IEEE) pp 227–32
- [18] Henstock M E and Spencer-Timms E S 1963 The composition of thin electrodeposited alloy films with special reference to nickel-iron *Proc. 6th Int. Metal Finishing Conf.* pp 179–85
- [19] Wolf W 1962 Electrodeposition of magnetic materials *J. Appl. Phys.* 33 1152–9
- [20] MacInnis R D and Gow K V 1971 Tensile strength and hardness of electrodeposited nickel-iron foil *Plating* 135–6